Energies **2015**, *8*, 8482-8496; doi:10.3390/en8088482

OPEN ACCESS

energies

ISSN 1996-1073

www.mdpi.com/journal/energies

Article

Measurements of the Aerodynamic Normal Forces on a 12-kW Straight-Bladed Vertical Axis Wind Turbine

Eduard Dyachuk *, Morgan Rossander, Anders Goude and Hans Bernhoff

Division of Electricity, Department of Engineering Sciences, Uppsala University, Box 534, Uppsala 751 21, Sweden; E-Mails: morgan.rossander@angstrom.uu.se (M.R.); anders.goude@angstrom.uu.se (A.G.); hans.bernhoff@angstrom.uu.se (H.B.)

* Author to whom correspondence should be addressed; E-Mail: eduard.dyachuk@angstrom.uu.se; Tel.: +46-18-471-5849.

Academic Editor: Frede Blaabjerg

Received: 5 June 2015 / Accepted: 3 August 2015 / Published: 12 August 2015

Abstract: The knowledge of unsteady forces is necessary when designing vertical axis wind turbines (VAWTs). Measurement data for turbines operating at an open site are still very limited. The data obtained from wind tunnels or towing tanks can be used, but have limited applicability when designing large-scale VAWTs. This study presents experimental data on the normal forces of a 12-kW straight-bladed VAWT operated at an open site north of Uppsala, Sweden. The normal forces are measured with four single-axis load cells. The data are obtained for a wide range of tip speed ratios: from 1.7 to 4.6. The behavior of the normal forces is analyzed. The presented data can be used in validations of aerodynamic models and the mechanical design for VAWTs.

Keywords: vertical axis turbine; wind turbine; force; measurement; accuracy; normal force; H-rotor; blades

---

1. Introduction

The majority of the wind turbines operating today are horizontal axis wind turbines (HAWT). However, there is a growing interest in vertical axis wind turbines (VAWT), which have the potential to reduce the cost of energy [1,2]. The concept of VAWTs has several advantages over the conventional HAWTs. Firstly, the generator of the VAWT can be placed at the ground level, and thus, the mass of the

generator is not of a concern. The lower center of gravity (compared to HAWTs) is specifically beneficial for the offshore floating platforms [3]. Secondly, VAWTs are omni-directional, and the yawing system is excluded. Thirdly, the size of the turbine rotor can be adjusted in two dimensions to meet the power needs: *i.e.*, both the diameter and height of the rotor can be changed for VAWTs, compared to HAWTs, where the rotor size is defined by its diameter. This is beneficial for the water current power applications, since the turbine size can be limited by both the width and depth of a channel. Several projects on large offshore VAWTs are currently being carried out [4–6].

One difficulty associated with VAWTs is the fluid dynamics, which is much more complex compared to the aerodynamics of HAWTs. For VAWTs with a fixed blade pitch, the angle of attack continuously changes with the blade position, and the dynamic stall event is present at lower tip speed ratios (TSR). Additionally, the blades of VAWTs interact with the incoming flow twice, both at the upwind and downwind sides of the rotor. The forces acting on the VAWT rotor vary during operation, and the blades are exposed to cyclic stress. Moreover, the cyclic forces on the blades affect the tower and the drive train. It is noted from previous studies that the unsteady loads are of a major concern for VAWTs [2].

Data on the measured forces for VAWTs are still limited. In the 1980s, Sandia National Laboratories conducted a series of experiments on large VAWTs with parabolic blades made of extruded aluminum [7–9]. The measured data on the Sandia 17-m turbine [8] are still widely used to validate simulation models, because of the turbine's size and the Reynolds number $\mathrm{Re} > 1 \times 10^6$ [10–12]. Other measurement data are available from small-scale vertical axis turbines tested in towing tanks with the Reynolds number of Re = 40,000 [13,14]. However up to date, there is a lack of measurement data on modern straight-bladed VAWTs operating at sufficiently high Reynolds numbers.

The present study is based on force measurements on the VAWT with the H-rotor, which is located north of Uppsala, Sweden (N 59°55′32”, E 17°35′12”). The VAWT was constructed in 2006, and it has mainly been used for studies on the electrical system [15,16]. A study on the power coefficient (C_P) of the turbine has been carried out in 2011 for the TSRs between 1.7 and 4.5 with the maximum C_P obtained at the TSR of 3.3 [15]. In 2014, the turbine was renovated, and load cells were installed for force measurements. The diameter of the turbine is 6.48 m with installed load cells, and the average Reynolds number during operation is $\mathrm{Re} > 0.5 \times 10^6$. The experimental method of the force measurements is described in [17]. The study has shown that the normal forces can be measured with the chosen method, but the tangential forces are disturbed by the turbine dynamics. Those disturbances are not connected to the aerodynamics, and the tangential forces are therefore not studied here. Hence, only data for the normal forces will be presented here.

The objective of the current study is to present experimental data on the normal forces on the straight-bladed VAWT operating at an open site at high Reynolds numbers. The normal forces response is analyzed for the wide range of operational conditions, including unsteady incoming wind flow.

2. Theory

The H-rotor is a lift-based machine, *i.e.*, the driving torque is generated by the lift force. Figure 1 shows the notations of the velocity vectors and forces acting on the blade of a VAWT. Due to the extracted

energy from the flow, the wind velocity at the blade, V, is generally lower than the asymptotic velocity, V_∞. The tangential velocity of the blade is:

$$V_\mathrm{b} = \Omega R \tag{1}$$

where Ω is the rotor angular velocity and R is the rotor radius. The relative wind velocity V_rel is the vector sum of the flow velocities at the blade. The angle of attack α is:

$$\alpha = \varphi + \delta \tag{2}$$

where φ is the angle of relative wind and δ is the blade pitch angle. The tip speed ratio (TSR) is:

$$\lambda = \frac{\Omega R}{V_\infty} \tag{3}$$

where V_∞ is the asymptotic wind velocity. Figure 1 shows the notations of the forces on a VAWT blade. F_L and F_D are lift and drag forces, and F_N and F_T are normal and tangential forces, respectively. Lift and drag forces can be defined through lift and drag coefficients, C_L and C_D:

$$F_\mathrm{L,D} = \frac{1}{2}\rho A_\mathrm{blade} \left|V_\mathrm{rel}\right|^2 C_\mathrm{L,D} \tag{4}$$

Here, ρ is the air density, A_blade is the blade area ($A_\mathrm{blade} = \int_0^H c(h)\,\mathrm{d}h$, where c is the blade chord length and H is the blade length). C_L and C_D are dependent on the airfoil type, the Reynolds number and the angle of attack α.

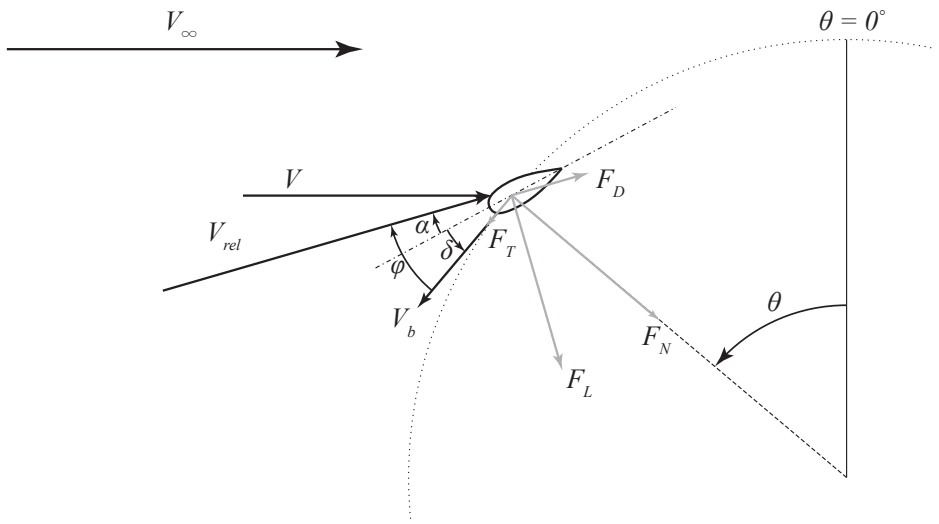

Figure 1. Definitions of the force and velocity vectors for vertical axis wind turbines (VAWTs). Angle θ is the blade azimuthal angle. The counter-clockwise direction is positive for the angles. Note that the angles α and φ are negative for the directions of V_b and V_rel in the figure. The positive direction of F_N is outwards from the turbine disk, *i.e.*, F_N in the figure is negative.

The tangential and normal forces are:

$$F_\mathrm{T} = F_\mathrm{L}\sin\varphi - F_\mathrm{D}\cos\varphi \tag{5}$$

$$F_\mathrm{N} = F_\mathrm{L}\cos\varphi + F_\mathrm{D}\sin\varphi \tag{6}$$

The normal force F_N gives the main structural loads on the blades, and the tangential force F_T is used when estimating a torque from the turbine.

For turbines with fixed blade pitch angle δ, the magnitude of the variations of the angle of attack α increases with decreased TSR. The lift coefficient C_L increases as α increases until the point of flow reversal within the boundary layer (known as the stall point). After the stall onset, the lift drops and the drag increases, which causes a drop in the torque driving force F_T, Equation (5), and the drag F_D becomes dominating for the normal force F_N, Equation (6). Since the angles of attack and the relative wind velocity at the blade continuously vary during the operation of VAWT, dynamic stall is present, which is characterized by the hysteresis behavior of the lift and drag coefficients. During the dynamic stall, the lift and drag coefficients become different from those in the static flow.

3. Experimental Setup

This section presents the experimental assembly for measuring the aerodynamic normal force on the turbine. The details on the measurement system and the experimental method together with the turbine dimensions are found in [17]. The 12-kW turbine used for the measurements is shown in Figure 2.

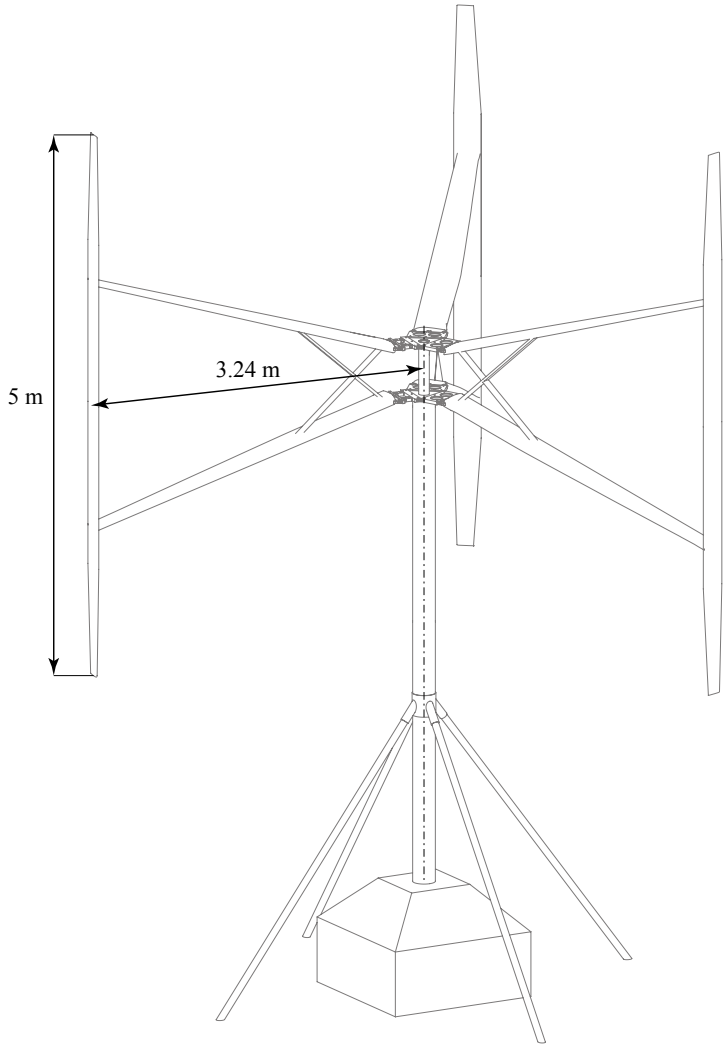

Figure 2. The VAWT with installed load cells.

The turbine radius is 3.24 m (with installed load cells), and the blade length is 5 m. The blades have the symmetrical profile NACA0021 with a chord length of 0.25 m at the mid-section and tapered ends. The tapering is used to reduce the induced drag. This should reduce the normal force close to the tip as the normal force is proportional to the chord according to Equations (4) and (6). This is beneficial from a structural point of view, as it reduces the bending moments in the blade. The tapering begins at 1 m from the ends, and the chord at the tip is 0.15 m. The blades have pitch angle $\delta = 2°$.

Figures 3 and 4 show force sensors, which are installed at the turbine's hub to measure the forces on the rotor. The force sensors are point load single-axis load cells, which measure tension and compression. The turbine rotational speed is controlled by controlling the electric load of the generator [15,17]. When the angular speed of the turbine is nearly constant, it can be assumed that the rate of change in angular momentum approaches zero, and centrifugal force on the rotor is constant. Based on this assumption and using the force notations and the dimensions from Figures 3 and 4, F_{N} is estimated as follows:

$$F_{\mathrm{N}} = F_0 + F_1 + F_2 + F_3 - F_{\mathrm{C}} \tag{7}$$

where F_{C} in Equation (7) is the centrifugal force, which is:

$$F_{\mathrm{C}} = m\Omega^2 L_{\mathrm{C}} \tag{8}$$

where m is the mass of the blade and support arms, m = 35.79 kg, L_{C} = 1.83 m.

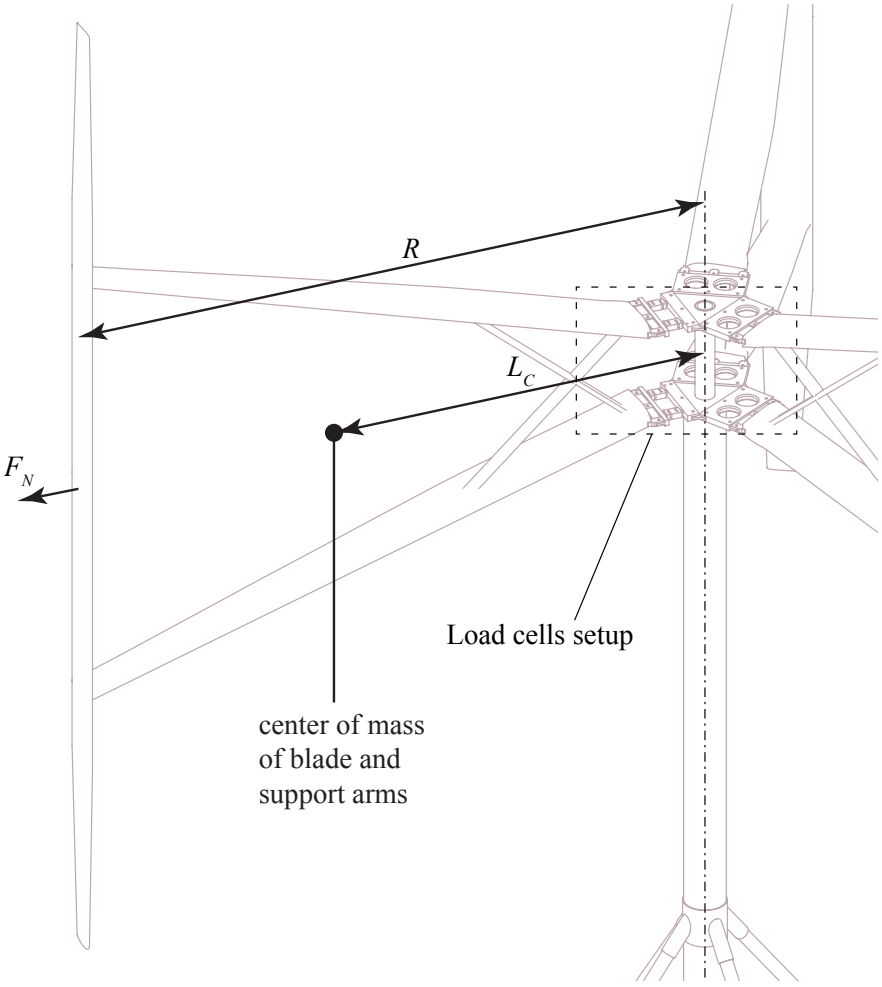

Figure 3. The turbine blade with installed load cells and the notation of the normal force F_{N}.

Wind speed and wind direction together with air temperature, air pressure and air humidity (used to estimate the air density) are measured at a weather station located 15 m from the turbine. The weather data are sampled at 1 Hz, and the force data are sampled at 2 kHz.

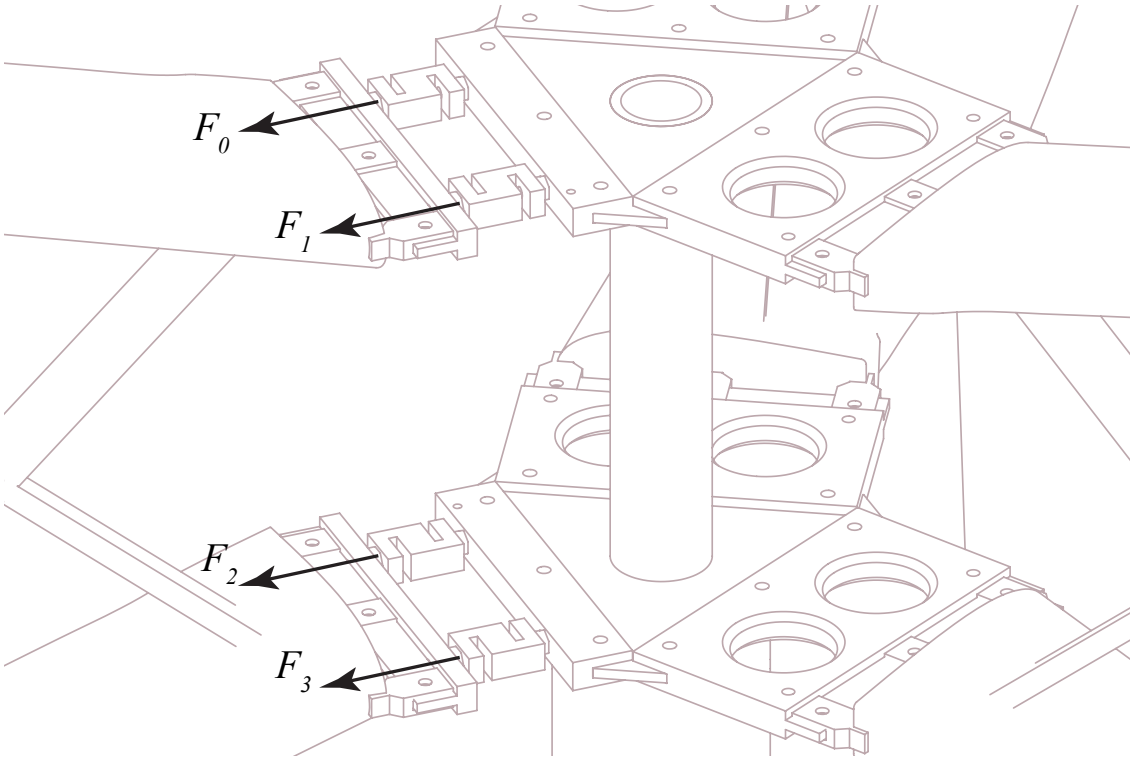

Figure 4. The notations of the measured loads.

3.1. Data Extraction

The measurement data were obtained from September to December 2014. Both wind speed and wind direction had large variations at the measurement site. Therefore, conditions of steady flow were defined to extract data bins. The time span of the steady conditions was divided into two parts: the time required to build a stable wake (further referred to as the "wake time"), followed by the time of steady flow operation (further referred to as the "disk time"). The wake time was set to 16 s (corresponding to 10 revolutions at 40 rpm), and the disk time was set to 8 s (5 revolutions at 40 rpm). The relative standard deviation (RSD) of the wind speed, wind direction and the turbine rotational speed during the wake and the disk time was used to extract data bins with steady conditions. The following expression for the RSD was used:

$$RSD = \left(\frac{1}{n} \sum_{j=1}^{n} \left(x_j - \langle x \rangle \right)^2 \right)^{\frac{1}{2}} \frac{1}{\langle x \rangle} \times 100\% \tag{9}$$

where $\langle x \rangle$ is:

$$\langle x \rangle = \frac{1}{n} \sum_{j=1}^{n} x_j \tag{10}$$

The flow was considered steady when the RSD of the wind speed V_∞ during the wake time was $\leq$10% and the RSD of V_∞ was $\leq$5% during the disk time; see Figure 5. Additionally, the RSD requirements of the wind direction Vdir and the turbine rotational speed Ω were $\leq$1% during both wake and disk time.

Obtained measured data were scanned to identify the bins, which met the aforementioned requirements of the maximum allowed RSD of V_∞, Vdir and Ω. These data bins were used in this work together with one data bin with higher allowed RSD of V_∞ and Vdir (defined as unsteady flow).

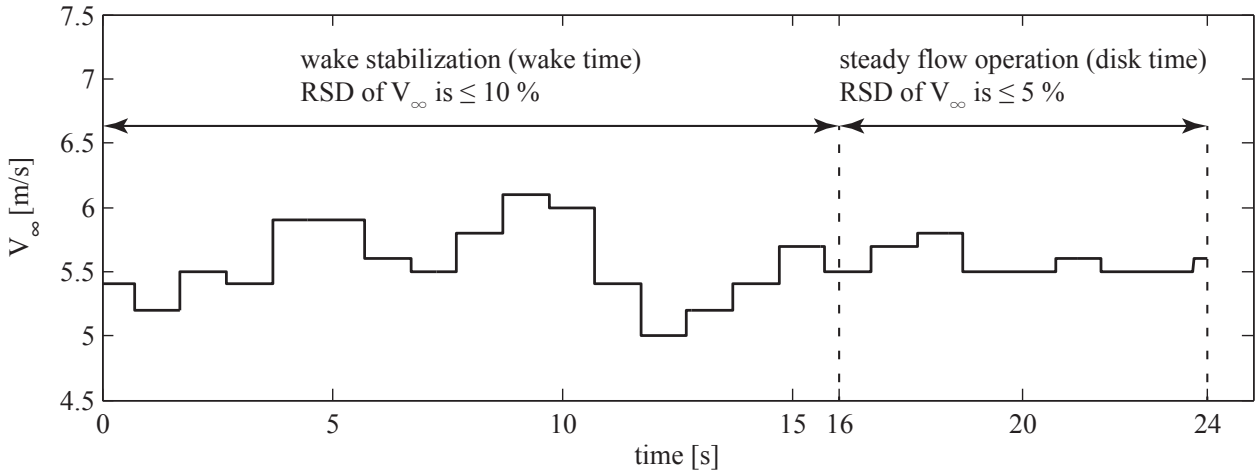

Figure 5. Allowed variations of the asymptotic wind speed during steady conditions. Illustration of the wake time and disk time.

4. Results and Discussion

The measurements during steady conditions are presented for a range of TSRs, from $\lambda = 1.7$ to $\lambda = 4.6$. The value of TSR is estimated using the average rotational speed Ω and the average wind velocity V_∞:

$$\lambda = \frac{\langle \Omega \rangle \, R}{\langle V_\infty \rangle} \tag{11}$$

where $\langle \Omega \rangle$ and $\langle V_\infty \rangle$ are averages taken over time with steady conditions. The turbine rotational speed is further referred to as $\langle \Omega \rangle$.

Since the wind speed varies with different TSRs, the normal force F_N is normalized, and the normal force coefficient C_N is determined as:

$$C_\mathrm{N} = \frac{F_\mathrm{N}}{0.5 \, \langle \rho \rangle \, A_\mathrm{blade} \, \langle V_\infty^2 \rangle} \tag{12}$$

where $\langle \rho \rangle$ is the average of the measured air density, $A_\mathrm{blade} = 1.15\,\mathrm{m}^2$ is the blade area and $\langle V_\infty^2 \rangle$ is the average squared asymptotic velocity. The asymptotic velocity V_∞ instead of the relative wind velocity V_rel is used in Equation (12), since V_rel is not measured. Please note that the averages of ρ and V_∞^2 are used in Equation (12), since ρ and V_∞ are measured 15 m away from the turbine, *i.e.*, a variation of ρ and V_∞ does not instantly correspond to a change in the measured normal force F_N.

4.1. Measurement Accuracy

Estimation of the maximum error of a value based on measurements can be performed as:

$$|\Delta Z| = \left|\frac{\partial Z}{\partial x}\Delta x\right| + \left|\frac{\partial Z}{\partial y}\Delta y\right| + \dots \tag{13}$$

where x, y, ... are measurements and Δx, Δy, ... are the maximum errors of the measurements. The maximum error of the normal force coefficient is estimated by applying Equation (13) on Equation (12):

$$\Delta C_{\mathrm{N}} = \left|\frac{\partial C_{\mathrm{N}}}{\partial \rho}\Delta\rho\right| + \left|\frac{\partial C_{\mathrm{N}}}{\partial A_{\mathrm{blade}}}\Delta A_{\mathrm{blade}}\right| + \left|\frac{\partial C_{\mathrm{N}}}{\partial V_{\infty}}\Delta V_{\infty}\right| + \left|\frac{\partial C_{\mathrm{N}}}{\partial F_{\mathrm{N}}}\Delta F_{\mathrm{N}}\right| \tag{14}$$

where $\Delta\rho = \pm 0.0016\,\mathrm{kg/m^3}$, $\Delta A_{\mathrm{blade}} = \pm 0.0016\,\mathrm{m^2}$ and $\Delta V_{\infty} = \pm 0.3\,\mathrm{m/s}$ are maximum errors of the air density, blade area and asymptotic wind velocity, specified in [17]. Please note that the maximum error ΔV_{∞} remains constant for the wind speed up to $10\,\mathrm{m/s}$. The maximum error of the normal force ΔF_{N} is dependent on the rotational speed of the turbine, and the expression for ΔF_{N} is given in [17]:

$$\Delta F_{\mathrm{N}} = \pm\left(0.0049\Omega_{\mathrm{rpm}}^2 + 0.072\Omega_{\mathrm{rpm}} + 23\right) \tag{15}$$

where Ω_{rpm} is the turbine rotational speed expressed in rpm. The maximum error of the shape of the normal force is $\Delta F_{\mathrm{N,shape}} = \pm 23$ N, as specified in [17]. The maximum error of the shape $\Delta F_{\mathrm{N,shape}}$ is independent of the accuracy of the measured centrifugal force F_{C}, and therefore, $\Delta F_{\mathrm{N,shape}}$ is lower than ΔF_{N}. The maximum error of the shape of the normal force coefficient $\Delta C_{\mathrm{N,shape}}$ is calculated as in Equation (14), but with $\Delta F_{\mathrm{N,shape}}$ instead of ΔF_{N}. Both ΔC_{N} and $\Delta C_{\mathrm{N,shape}}$ depend on the normal force, wind speed and air density. ΔC_{N} is further dependent on the accuracy of the measured L_{C} and the turbine rotational speed Ω_{rpm}, which are used to estimate the centrifugal force F_{C}. The maximum error in the measured TSR is estimated based on Equations (11) and (13):

$$\Delta\lambda = \left|\frac{\partial\lambda}{\partial\Omega}\Delta\Omega\right| + \left|\frac{\partial\lambda}{\partial R}\Delta R\right| + \left|\frac{\partial\lambda}{\partial V_{\infty}}\Delta V_{\infty}\right| \tag{16}$$

where $\Delta\Omega = \pm 0.0052$ rad/s and $\Delta R = \pm 0.01$ m are maximum errors of the measured rotational speed and turbine radius, which are specified in [17].

4.2. Normal Force Coefficient

Time series of C_{N} and the maximum error ΔC_{N} for steady wind conditions are shown in Figure 6 together with the measured wind speed V_{∞}, the wind direction $V\mathrm{dir}$ and the turbine rotational speed Ω. The variations of V_{∞}, $V\mathrm{dir}$ and Ω are within the limits described in Section 3.1.

This is compared against the time series during unsteady wind conditions, where the variations of V_{∞}, $V\mathrm{dir}$ and Ω are considerably higher than the limits for steady conditions (Figure 7). Estimation of the TSR for the unsteady wind is done with Equation (11) to compare the C_{N} response at steady flow against the unsteady flow. The oscillations of C_{N} at the unsteady wind are present at both upwind and downwind sides of the rotor for each revolution, while the C_{N} response at the steady wind has less variations. Such a difference in C_{N} oscillations is due to the varying wind flow. The wind speed variations are ± 0.2 m/s

and ± 1.0 m/s for the steady and the unsteady wind, correspondingly, and the variations in wind direction are within $\pm 2^\circ$ and $\pm 7^\circ$ for the steady and the unsteady conditions respectively.

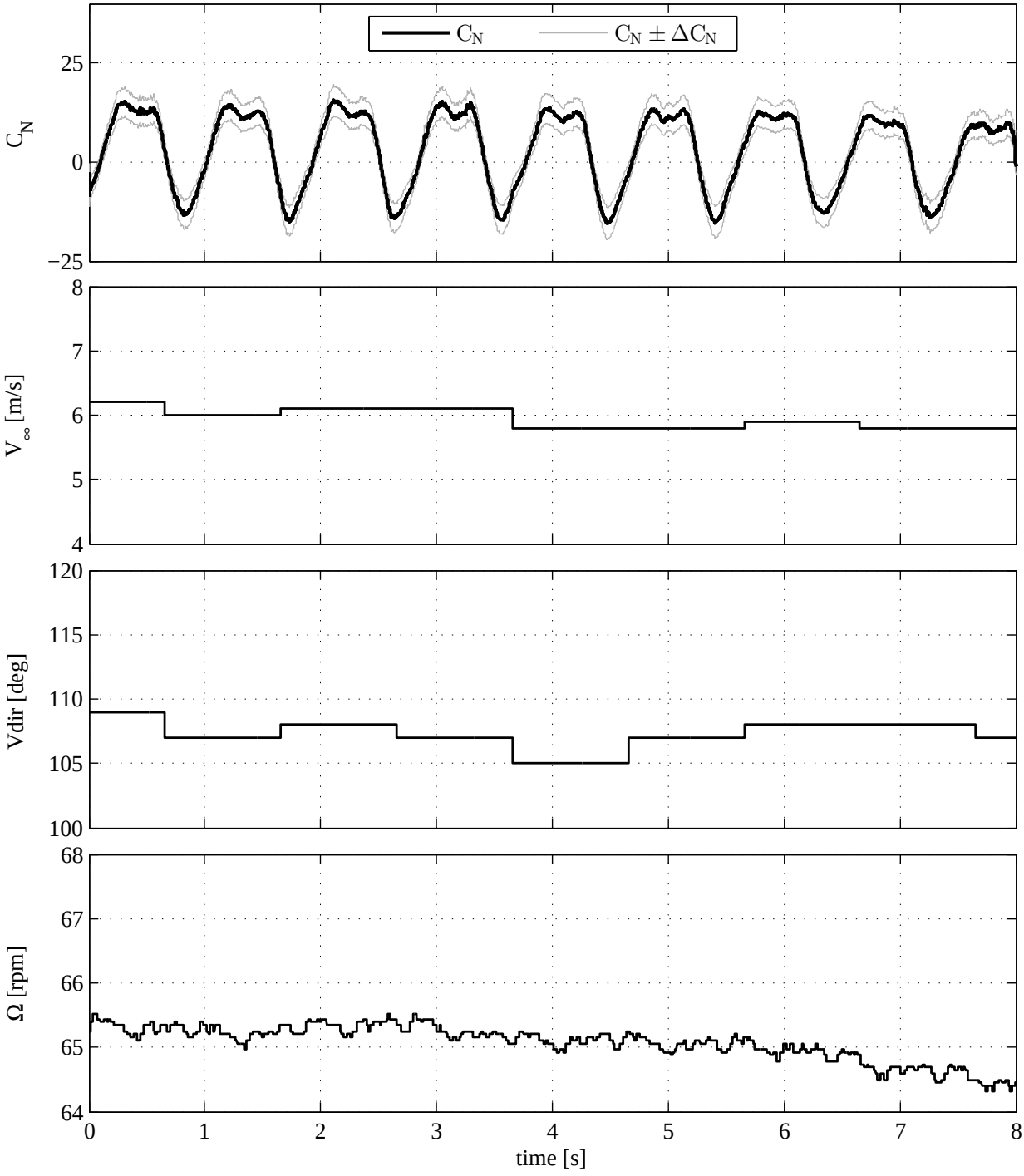

Figure 6. Normal force coefficient, wind speed, wind direction and the turbine rotational speed at steady wind conditions, $\lambda = 3.7$, $\langle \Omega \rangle = 65$ rpm.

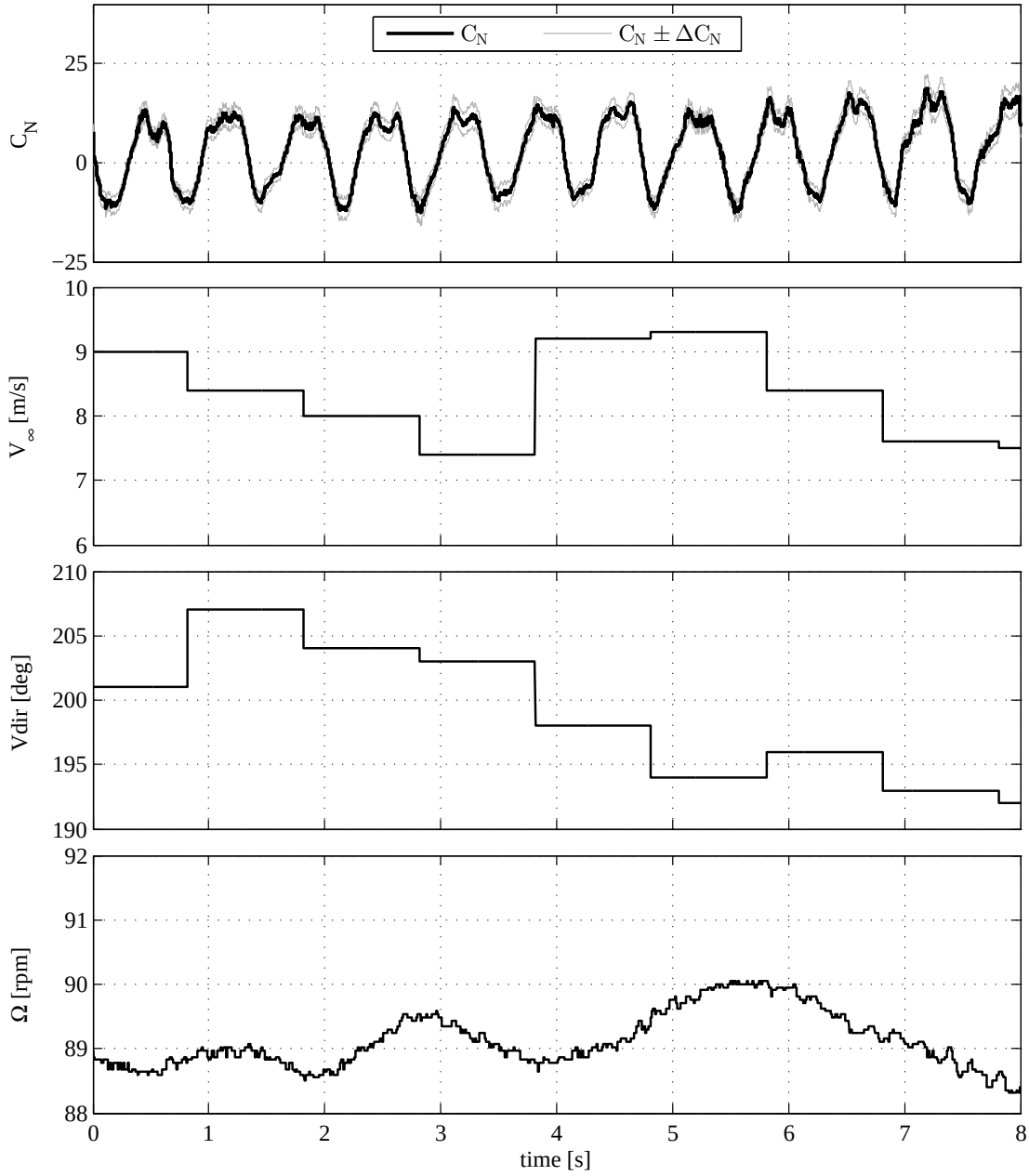

Figure 7. Normal force coefficient, wind speed, wind direction and the turbine rotational speed at unsteady wind conditions, $\lambda = 3.6$, $\langle\Omega\rangle = 89$ rpm. Note that V_∞ is measured 15 m away from the turbine.

However, even for the unsteady conditions, the force data are periodic and have less high-frequency components. The maximum measurement errors of TSR and C_N together with the average air density are presented in Table 1. Note that the maximum error ΔC_N is larger than the maximum error of the shape $\Delta C_\mathrm{N,shape}$, as described in Section 4.1. The presented figures show higher maximum measurement errors for the steady wind conditions. The reason is that for the presented data, the wind speed and the turbine rotational speed are higher at the unsteady conditions than at the steady conditions, and therefore, according to Equations (14)–(16), the maximum errors $\Delta\lambda$, ΔC_N and $\Delta C_\mathrm{N,shape}$ decrease with increased V_∞ and Ω. Please note that the current estimation method of $\Delta\lambda$, ΔC_N and $\Delta C_\mathrm{N,shape}$ assumes that

the flow velocity at the anemometer and the turbine are fully correlated. For steady conditions, this should be a valid approximation. However, for the unsteady conditions, the correlation between V_∞ at the anemometer and the turbine decreases, which is not included in the presented method of the error estimation. Hence, the maximum errors $\Delta\lambda$, ΔC_N and $\Delta C_{N,shape}$ are most likely to be higher for the unsteady conditions, as they depend on ΔV_∞.

Table 1. Summary of the results and maximum measurement errors. Note that λ at the unsteady conditions is estimated with Ω and V_∞, which have higher variations than the variations for the steady conditions; Section 3.1.

Conditions	λ	$\langle\Omega\rangle$ (rpm)	max ΔC_N	max $\Delta C_{N,shape}$	$\langle\rho\rangle$ (kg/m^3)
Steady, Figure 6	3.71 ± 0.20	65.07	±4.0	±3.0	1.2385
Unsteady, Figure 7	3.61 ± 0.14	89.13	±3.6	±2.5	1.2469
65 rpm, Figure 8	3.06 ± 0.14	65.36	±2.4	±1.7	1.2367
	3.87 ± 0.22	65.98	±4.1	±3.0	1.2447
	4.57 ± 0.30	65.35	±5.7	±4.2	1.2479
50 rpm, Figure 9	2.55 ± 0.13	49.89	±2.0	±1.5	1.2535
	3.04 ± 0.18	49.74	±3.2	±2.5	1.2748
	3.88 ± 0.28	49.57	±5.3	±4.2	1.2761
40 rpm, Figure 10	1.66 ± 0.07	39.97	±1.2	±1.0	1.2533
	1.84 ± 0.08	40.29	±1.5	±1.2	1.2533

Figures 8–10 present the C_N response during one revolution, which is taken as the average of five revolutions at steady conditions (Section 3.1). The standard deviation σ is presented, which is obtained as the standard deviation of the C_N response in each position of the five revolutions.

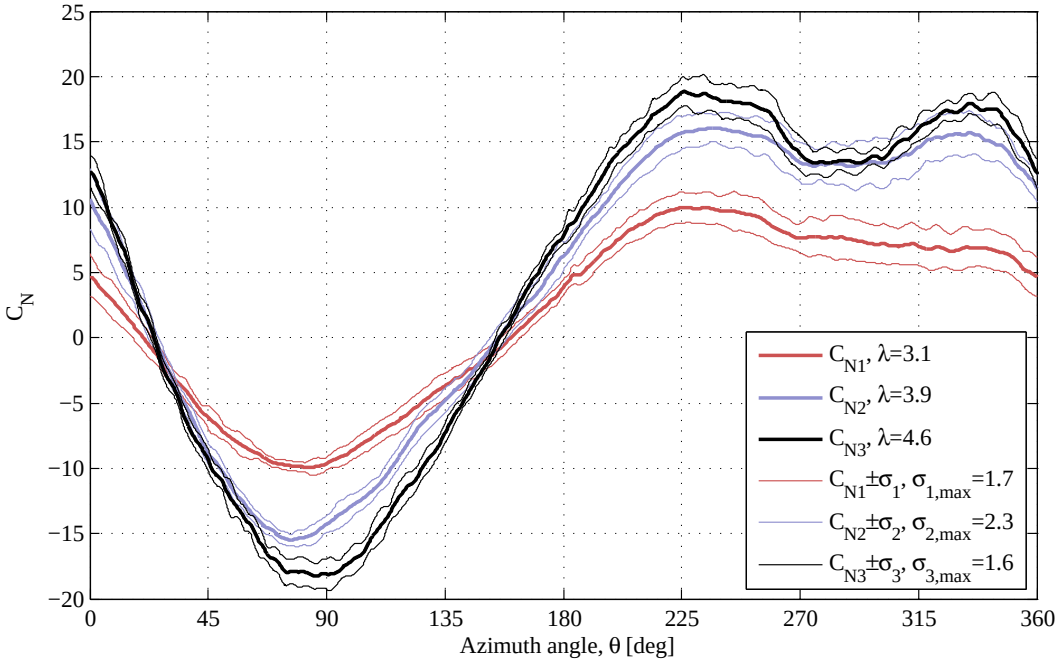

Figure 8. The average normal force coefficient at the turbine rotational speed of 65 rpm.

The maximum measurement errors of $\Delta\lambda$, ΔC_{N} and $\Delta C_{\mathrm{N,shape}}$ together with the measured air density are presented in Table 1. The difference in TSR between the datasets is due to the change in the asymptotic velocity since the turbine was operated at constant rotational speed.

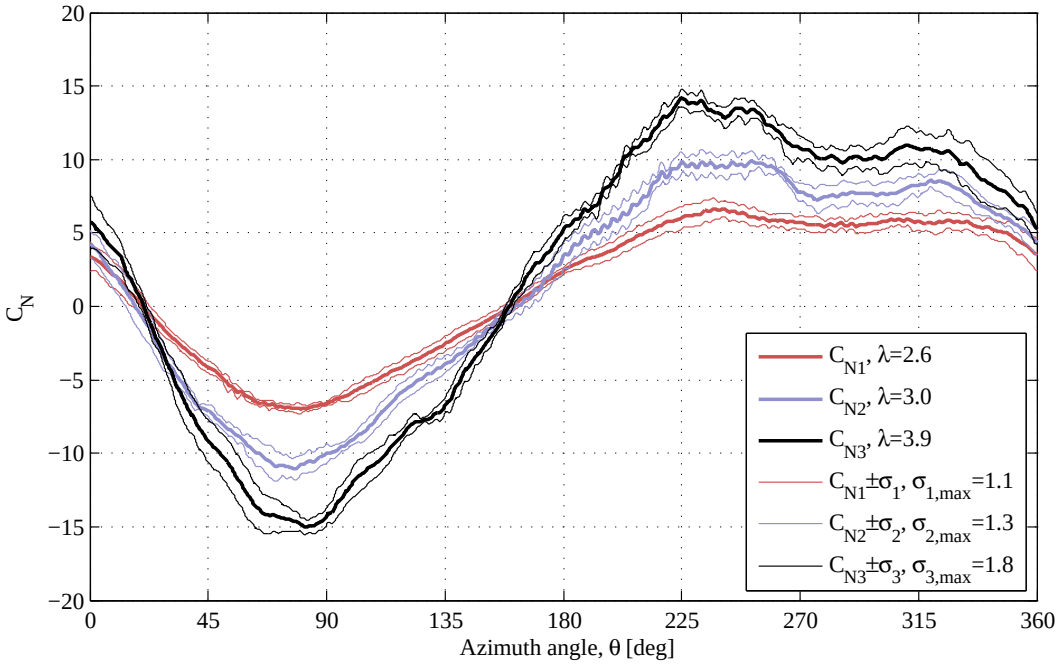

Figure 9. The average normal force coefficient at the turbine rotational speed of 50 rpm.

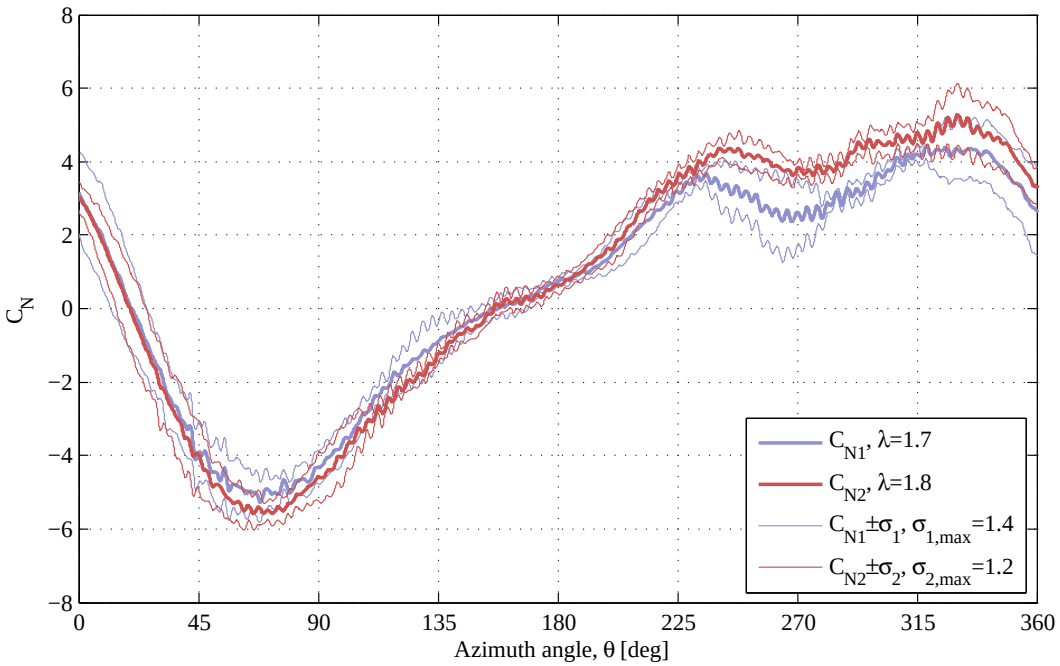

Figure 10. The average normal force coefficient at the turbine rotational speed of 40 rpm.

The results in Figures 8–10 show the repeatability of the C_{N} response during steady conditions, which is seen from the standard deviation σ. Therefore, the trends are most likely accurate, even though the measurements error can cause a shift in the scale of the C_{N} response. The C_{N} response has smaller

deviations at the upwind region compared to the downwind region, which likely is an effect of the wake in the downwind region.

The blade pitch angle δ influences the angle of attack α and is used to decrease the dynamic stall effect by evening out the magnitudes of α between the upwind and downwind regions. The influence of the blade pitch is observed in the results as an increase in the values of C_N, which is the reason why the magnitude of C_N is similar between the upwind and the downwind sides (Figures 8 and 9). The positive offset of the C_N response at $\theta = 0°$ is the consequence of both the blade pitch and flow expansion, and it is present for all of the C_N curves. The downwind region of the C_N response is wider than the upwind region at higher TSRs, which corresponds to the flow expansion. Additionally, it is noted that the magnitude of the C_N response increases with increased TSR, which is expected with normalization based on the asymptotic wind velocity V_∞ (Equation (12)).

One interesting phenomenon is that there is a drop in the C_N response at TSRs of 3.9 and 4.6 in the downwind region at $250° < \theta < 330°$, which is less pronounced at a TSR of 3.1 (Figure 8). The drop in C_N at the downwind region is present at a rotational speed of 50 rpm at TSRs of 3.0 and 3.9 (Figure 9), though in a more narrow region compared to the one at 65 rpm. The drop in C_N is also present when operating the turbine at low TSRs at the rotational speed of 40 rpm (Figure 10). The region of the C_N-drop for the speed of 40 rpm is shifted to $240° < \theta < 310°$, when comparing to higher TSRs at 50 rpm and 65 rpm. The C_N-drop at low TSRs has been observed in the experimental studies on VAWTs with parabolic blades [8]; however, a C_N-drop at high TSRs has not been noted before. The C_N-drop is not likely due to the tower wake, since the tower diameter is significantly smaller than the region of the C_N-drop. The authors presume that the C_N-drop is either due to the wake of the support arms or because the blade interferes with the tip vortices released at the upwind side.

4.3. General Comments

The presented data show trends that have not been observed in the previously measured data on VAWTs with parabolic blades [8]. The examples are the flow expansion and the C_N-drop in the downwind. The flow expansion is present at high rotational speed and high TSR, while it is not observed in [8]. This can be due to the different experimental methods. The sensors in [8] were installed at the mid-blade, and thus, the forces were measured in two-dimensional space. With the current experimental method [17], the forces are obtained in three-dimensional space. Additionally, a drop in the C_N response is observed at the downwind region at both steady and unsteady conditions. Finally, it is important to note that the presented measurements of C_N include the contribution of the support arms of the turbine, *i.e.*, it is not a measurement on the turbine blades solely.

5. Conclusions

The results on the turbine loads are presented together with the measurement accuracy, and the range of TSRs from $\lambda = 1.7$ to $\lambda = 4.6$ is studied. The behavior of the measured normal force is consistent within the turbine revolution, and it is analyzed for all of the tested conditions. Additionally, a comparison of the normal force for several revolutions during steady and unsteady wind conditions is presented. It is shown that the normal force response is periodic at the unsteady wind. The presented results of the normal force

variations can be used for mechanical design and for validating simulation models of VAWTs. However, the results should be applied when studying the whole turbine and not only the blades, because the support arms contribute to the measured normal force, as well.

Acknowledgments

The authors would like to acknowledge the J. Gust Richert foundation for the financial contribution to the equipment for the experiment. This project is conducted with the support of STandUP for Energy. Dana Salar is acknowledged for the help with the modification of the turbine.

Author Contributions

Eduard Dyachuk obtained the results from the measurement data and wrote the article. Morgan Rossander was responsible for the experimental campaign and for the measurement error estimation. Eduard Dyachuk and Anders Goude analyzed the data. Hans Bernhoff was the main supervisor of the project.

Conflicts of Interest

The authors declare no conflict of interest.

References

1. Paquette, J.; Barone, M. Innovative offshore vertical-axis wind turbine rotor project. In Proceedings of EWEA 2012 Annual Event, Copenhagen, Denmark, 16–19 April 2012.
2. Sutherland, H.J.; Berg, D.E.; Ashwill, T.D. *A Retrospective of VAWT Technology*; Technical Report SAND2012-0304; Sandia National Laboratories: Albuquerque, NM, USA, 2012.
3. Blusseau, P.; Patel, M.H. Gyroscopic effects on a large vertical axis wind turbine mounted on a floating structure. *Renew. Energy* **2012**, *46*, 31–42.
4. Paulsen, U.S.; Madsen, H.A.; Hattel, J.H.; Baran, I.; Nielsen, P.H. Design Optimization of a 5 MW Floating Offshore Vertical-Axis Wind Turbine. In Proceedings of the 10th Deep Sea Offshore Wind R and D Conference, DeepWind, Trondheim, Norway, 24–25 January 2013; Elsevier BV: Trondheim, Norway, 2013; Volume 35, pp. 22–32.
5. Shires, A. Design optimisation of an offshore vertical axis wind turbine. *Proc. ICE-Energy* **2013**, *166*, 7–18.
6. Kaldellis, J.; Kapsali, M. Shifting towards offshore wind energy—Recent activity and future development. *Energy Policy* **2013**, *53*, 136–148.
7. Johnston, S.F. *Proceedings of the Vertical Axis Wind Turbine (VAWT) Design Technology Seminar for Industry*; Technical Report SAND80-0984; Sandia National Laboratories: Albuquerque, NM, USA, 1982.
8. Akins, R.E. *Measurements of Surface Pressures on an Operating Vertical-Axis Wind Turbine*; Technical Report SAND89-7051; Sandia National Laboratories: Albuquerque, NM, USA, 1989.

9. Oler, J.; Strickland, J.; Im, B.; Graham, G. *Dynamic Stall Regulation of the Darrieus Turbine*; Sandia National Laboratories: Albuquerque, NM, USA, 1983.
10. Shires, A. Development and Evaluation of an Aerodynamic Model for a Novel Vertical Axis Wind Turbine Concept. *Energies* **2013**, *6*, 2501–2520.
11. Keinan, M. A Modified Streamtube Model for Vertical Axis Wind Turbines. *Wind Eng.* **2012**, *36*, 145–180.
12. Wang, K.; Hansen, M.O.L.; Moan, T. Model improvements for evaluating the effect of tower tilting on the aerodynamics of a vertical axis wind turbine. *Wind Energy* **2015**, *18*, 91–110.
13. Strickland, J.H.; Webster, B.T.; Nguyen, T. A vortex model of the Darrieus turbine: An analytical and experimental study. *J. Fluids Eng.* **1979**, *101*, 500–505.
14. Ashuri, T.; van Bussel, G.; Mieras, S. Development and validation of a computational model for design analysis of a novel marine turbine. *Wind Energy* **2013**, *16*, 77–90.
15. Kjellin, J.; Bülow, F.; Eriksson, S.; Deglaire, P.; Leijon, M.; Bernhoff, H. Power coefficient measurement on a 12 kW straight bladed vertical axis wind turbine. *Renew. Energy* **2011**, *36*, 3050–3053.
16. Apelfröjd, S.; Bülow, F.; Kjellin, J.; Eriksson, S. Laboratory verification of system for grid connection of a 12 kW variable speed wind turbine with a permanent magnet synchronous generator. In Proceedings of the EWEA 2012 Annual Event, Copenhagen, Denmark, 16–19 April 2012.
17. Rossander, M.; Dyachuk, E.; Apelfröjd, S.; Trolin, K.; Goude, A.; Bernhoff, H.; Eriksson, S. Evaluation of a blade force measurement system for a vertical axis wind turbine using load cells. *Energies* **2015**, *8*, 5973–5996.